International Journal of Electronics and Applied Research (IJEAR) **vol. 5, issue 1, June 2018**
Online (*http://eses.net.in/online_journal.html*) ISSN 2395-0064

Design And Analysis of Coplanar Waveguide Band Stop Filter Using Asymmetric Defected Ground Structure For Fine Alteration of Stop band

M.G. Kulkarni[1], A. N. Cheeran[2], K. P. Ray[3], S. S. Kakatkar[4]
[1]*K. J. Somaiya College of Engineering , Mumbai and Research Scholar, Veermata Jijabai Technological Institute (VJTI), Mumbai-400019, India, makarandkulkarni@somaiya.edu.*
[2]*Veermata Jijabai Technological Institute (VJTI), Mumbai-400019, India, ancheeran@vjti.org.*
[3]*Defence Institute of Advanced Technology (DIAT), Ministry of Defence, Govt. of India, Girinagar, Pune-411025, India, kpray@rediffmail.com.*
[4]*Society for Applied Microwave Electronics Engineering and Research (SAMEER), IIT Bombay Campus, Mumbai-400076, India, sskakat@gmail.com.*

Abstract

In this work, design and analysis of four configurations of band stop filter (BSF) has have been carried out based on coplanar waveguide (CPW) using rectangular dumbbell shaped 'Asymmetric Defected Ground Structure (ADGS)'. Asymmetries have been presented by varying the width of lower head of rectangular dumbbell shaped DGS to achieve the fine alteration in the stop bandwidth of BSF. The proposed CPW- BSF is easy to fabricate due to simple DGS geometry, and also easily modeled in terms of parallel R, L and C circuit to evaluate its theoretical filter response using ABCD parameters. This simulation analysis shows that fine alteration of stop bandwidth ranging from 350 MHz to 430 MHz, can be achieved . This CPW-BSF has filter selectivity better than 45 dB/GHz and radiation losses not more than 12.8 % with good sharpness factor near to unity, as desired. The measured results of the fabricated CPW-BSF using proposed ADGS show good agreement with its simulated results.

Key words*: 1. Asymmetric Defected Ground Structure, 2.Bandstop Filter, 3. Coplanar Waveguide, 4. Stopband, 5. Sharpness Factor*

1. Introduction

The lowermost part of the atmosphere, the PBL being in touch with the surface is affected by the solar energy input and consequent regular temperature variations of day and night and season and due to other

factors as cloud, aerosols etc. [Stull 33 1988, Arya 2009].Therefore the consequent thermodynamic activities of the earth surface are reflected most prominently in this layer. Normally the advent of the day increases surface temperature initiating uplift of warm gases and the mixing process begins. With the rise of temperatures the convection of warm gases generates thermal turbulence and energy transfer processes that breaks the boundary layer. This thermodynamic process remains active throughout the troposphere and continues during the sun light hours. With the sunset the reverse processes of cooling the earth surface by radiation begins and with this the thermal radiation from the surface initiates a different thermodynamic process of reversal of the mixing process triggering formation of thermal and mechanical irregularity structures and reestablishment of the PBL and other night time features of the surface layer.

Above the boundary layer the part of the atmosphere is isolated from the surface layer and normally remains relatively isolated from the layer below PBL. Therefore the troposphere may be divided into two parts, the planetary boundary layer (PBL) and the free troposphere which is the rest of the troposphere above it. In the free troposphere the rapid and relatively sharp temperature variations are not very significant. Because in that layer effects of earth surface temperature, moisture and heat exchange through mixing processes etc. experienced in the BL is not significant. However on special cases of presence of jet streams, heat/cold fronts etc the free atmospheric fluctuations may be significant. Turbulence is one of the important transport processes and it is used to define the boundary layer definition. The atmospheric boundary layer plays a very important role in the transport of momentum, moisture and energy through processes that are inherently turbulent. The turbulent flow in the atmospheric boundary layer can effectively transport moisture, momentum and energy through turbulent eddies.

During recent years, there has been emphasis on understanding the boundary layer height dynamics through analysis of temperature, potential temperature and specific humidity profiles, which are obtained from radiosonde ascents [Hooper and Eloranta 1986]. There are also several remote-sensing devices such as the light detection and ranging (LiDAR), sound detection and ranging (SoDAR), radio acoustic sounding system (RASS), GPS occultation measurements [Basha and Ratnam 2009; Xie et al. 2012] and radio wind profilers (RWP) have become indispensable tools to probe the atmospheric boundary layer and the troposphere within the first few kilometers above the ground.

Band stop filter (BSF) plays an important role in microwave and wireless applications like pocket and laptop computers, smart mobile phones, automobile navigators, and many wireless consumer devices. In this paper, BSF has been designed using the Coplanar Waveguide (CPW) proposed by C.P. Wen in 1969

[Wen. 1969]. Compared with microstrip structures, the CPW structures are more attractive because they require only a single metallization layer and offer greater design flexibility as well as ease of fabrication.

Filter can be implemented with shunt stubs or stepped-impedance lines in a microwave circuit [Pozar D. 2010]. The stepped-impedance filters are popular because they are easier to design and take comparatively lesser space than similar filters using stubs. But their electrical performance is not good. To implement any fine change in the stop bandwidth of filter, the complete design procedure needs to be repeated and hence it's time consuming. Also, the conventional design requires a larger circuit size which limits its applications and hence it is not useful in portable microwave and wireless communication systems. The BSF implemented using defected ground structure (DGS) has number of attractive features like small size, simple geometry, and deeper stop-band than that of a conventional filters, low insertion loss, and easy circuit modeling [Ahn et al. 2001]. In addition to filters, DGS is beneficial in many other microwave applications such as power dividers/couplers and amplifiers.

Cascading the DGS units called as Electromagnetic Band Gap (EBG) structures, can help to increase the stop bandwidth of BSF as per the requirements. CPW-BSF has been designed using EBG with double periodicity and T-shaped capacitive load located at periodic positions with strip width modulation reported by [Martine et al. 2003]. However, it required larger PCB area and had a limitation in microwave integrated circuit (MIC) applications. Few more complex EBG structures has presented by [Zoul et al. 2006]. A CPW-BSF with periodic cascading of four spiral DGS has been reported by [Lim et al. 2002]. Nevertheless, it results in narrow rejection bandwidth. Also, cascading of complicated spiral DGS geometry adds difficulty to maintain accuracy in fabrication. The CPW filter have presented by [Yun and Chang 2001] using symmetric square dumbbell DGS which gives wide stop bandwidth but higher radiation losses. In the previous work by the same authors [Kulkarni et al. 2017], the CPW band reject filter has been presented using the cascading arrangement of rectangular dumbbell shaped DGS, resulting wide rejection bandwidth, less radiation losses with improvements in overall filter performance. However all the reported work [Martine et al. 2003; Zoul et al. 2006; Lim et al. 2002; Kulkarni et al. 2017] does not give any solution to incorporate fine alteration of the stop bandwidth of BSF. Rectangular dumbbell DGS (RDDGS) was explored for the first time by [Ahn et al. 2001] for design a filter on microstrip lines. An asymmetric CPW-based structure has reported by [Naqui et. al. 2016] where the CPW central strip is kept unaltered whereas slotted DGS stepped impedance resonators are etched on ground planes in conventional CPW, to use it as a biological sensor. Three configurations of BSF have been presented

using CPW-DGS, Asymmetric CPW (ACPW)-DGS, and ACPW-ADGS filters by [Li 2014], in which to design of ACPW a conformal mapping technique has been used. In the earlier work by the same authors [Kulkarni et al. 2016], two CPW filter configurations have proposed. One is CPW with 'Symmetric DGS (SDGS)', in which upper and lower heads of rectangular dumbbell DGS has been made symmetric in size, and the second is CPW with 'Asymmetric DGS (ADGS)', in which lengths of upper and lower heads of DGS have been made asymmetric. However, the simulation as well as the measured results of the fabricated CPW-ADGS BSF show significant radiation loss (≈13 %) and also low filter selectivity (≈ 29 dB/GHz) [Kulkarni et al. 2016]. In order to obtain fine alteration in stopband and improvement in overall filter performance, the design and analytical study of CPW-BSF with new asymmetric DGS (CPW-ADGS) has been designed and analyzed in this work. In the proposed study of the CPW-BSF, only the width of lower head of rectangular dumbbell DGS have been made asymmetric in order to get two nearby transmission zeros which results in two resonance frequencies. By changing only the width of lower head of rectangular dumbbell DGS, positions of the transmission zeros at resonance frequencies and hence the stop bandwidth have been controlled. To examine the fine alteration in the stop bandwidth, four different design cases of CPW-BSF using ADGS have been analyzed here. The overall performance analysis of all these filters have been carried out in terms of cut-off frequency at -3 dB, resonant frequency, stop bandwidth at -10 dB, filter selectivity, sharpness factor, etc. The performance of the proposed CPW-BSF also has been compared with the earlier reported filters [Li 2014; Kulkarni et al. 2016]. Based on the overall comparative performance analysis, the optimum design of CPW-BSF has been fabricated and tested on vector network analyzer. The measured results of the fabricated CPW-BSF have been compared with its simulated and theoretical results.

2. Methodology

In this section, design of conventional CPW transmission line, CPW-BSF using SDGS, and ADGS which has been reported earlier, and the new four proposed design configurations of CPW-BSF using ADGS have been described. The substrate material of $\varepsilon_r = 4.5$, $\tan\delta = 0.002$, with thickness of 1.6 mm, has been used.

2.1 Design of Conventional CPW transmission line:

As shown in Figure 1, the CPW transmission line of characteristic impedance Z_0 = 50 Ω has been designed at 2.5 GHz, with a length of 40.2 mm, strip width of S = 6 mm, and gap spacing of W = 0.5 mm.

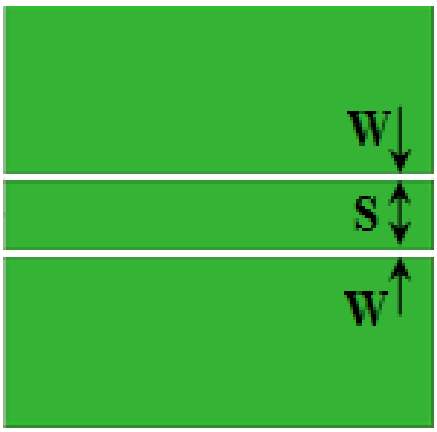

Figure 1: CPW Transmission Line

2.2 Designs of CPW-BSF using SDGS and ADGS:

In the earlier reported work by the same authors [Kulkarni et al. 2016], two CPW filter configurations have proposed. One is CPW-BSF using 'Symmetric DGS (SDGS)', as shown in Figure 2, in which upper and lower heads of rectangular dumbbell DGS has been made symmetric in size, and the second is CPW-BSF using 'Asymmetric DGS (ADGS)', as shown in Figure 3, in which lengths of upper and lower heads of DGS have been made asymmetric. However, the simulation as well as the measured results of the fabricated CPW-ADGS filter show significant radiation loss (≈13 %) and also low filter selectivity (≈ 29 dB/GHz).

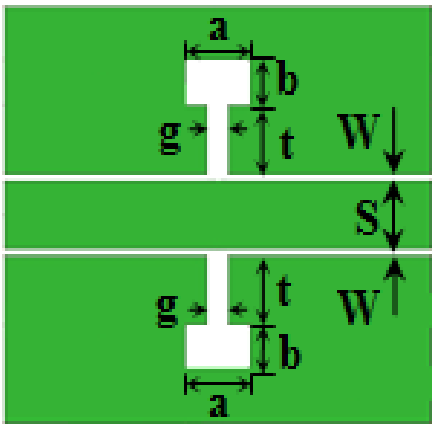

Figure 2: CPW-BSF using SDGS (a = 6 mm, b = 3.92 mm, g = 2 mm, t = 6 mm)

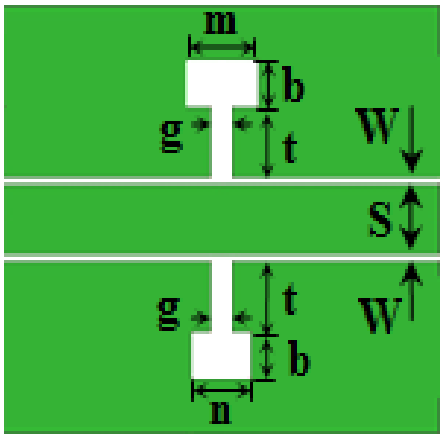

Figure 3: CPW-BSF using ADGS (m = 6.6 mm, n = 5.4 mm)

2.3 Design of CPW-BSF using proposed ADGS:

In this work, four design configurations of the proposed CPW-BSF using new ADGS are shown in Figure 4 to Figure 7. By varying the width of lower dumbbell head of DGS from b_1 to b_4, the four different configuration cases designated respectively as *Case 1* to *Case 4*, have been examined. The total PCB size for each of these configurations including designs shown in the section 2.1 and 2.2 is 40.2 mm × 36 mm

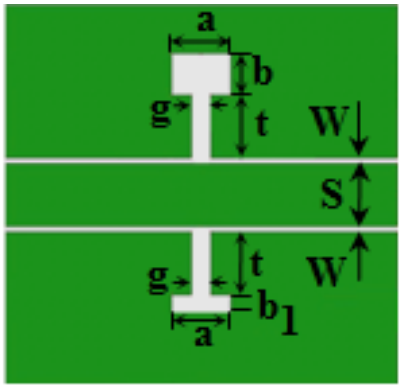

Figure 4: CPW-BSF using ADGS (b_1 = 2.5 mm)

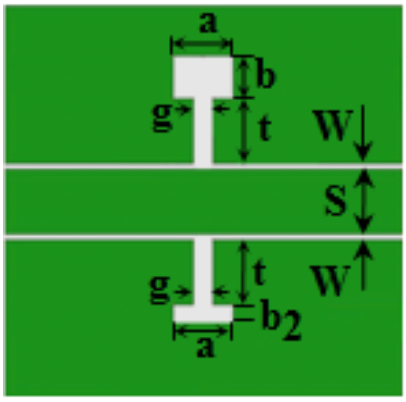

Figure 5: CPW-BSF using ADGS (b_2 = 2 mm)

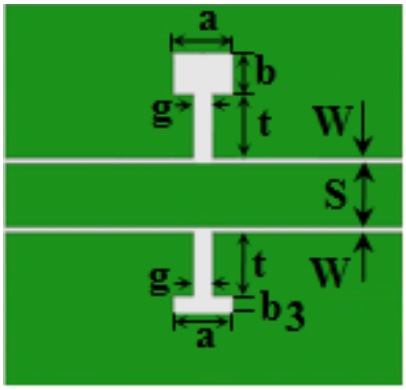

Figure 6: CPW-BSF using ADGS (b_3 = 1.8 mm)

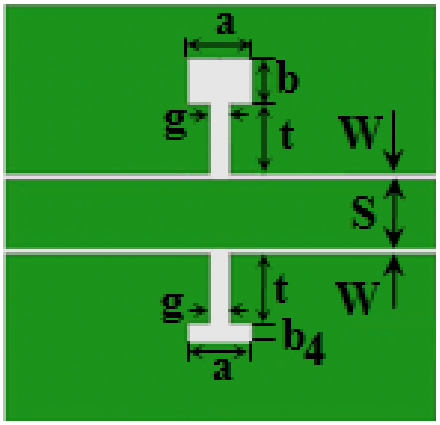

Figure 7:CPW-BSF using ADGS (b_4 = 1.5 mm)

3. Circuit Modeling And Result Analysis:

Figure 8 shows the equivalent circuit model of DGS unit [Lin et al. 2006], which consists of the parallel combination of Resistor (*R*), Inductor (*L*), and Capacitor (*C*), elements connected in series with the transmission line of electrical length '*kd / 2*' on both sides. Here, '*k*' is the propagation constant along the line without DGS and the physical length of the transmission line is '*d*'. The capacitance is due to stored charges at the gap. The inductance comes from the additional magnetic flux flowing through the two apertures, and the radiation effect is modeled by resistance. The *R*, *L*, and *C* elements can be calculated using (1-3) [Lin et al. 2006]. The asymmetric DGS can be modeled using series combination of two parallel *R*, *L*, *C* resonators, since its transfer characteristic has two different resonance frequencies at two transmission zeros as observed here. Here, the resistance R_i, inductance L_i and the capacitance C_i have been extracted and listed in Table I, where i = 1, for first resonance frequency (f_{01}) and i = 2, for second resonance frequency (f_{02}). After calculating *ABCD* parameters from (4) and (5) [Chang and Lee 2002], now it is possible to obtain scattering parameters, using (6) and (7) [Kulkarni et al. 2016].

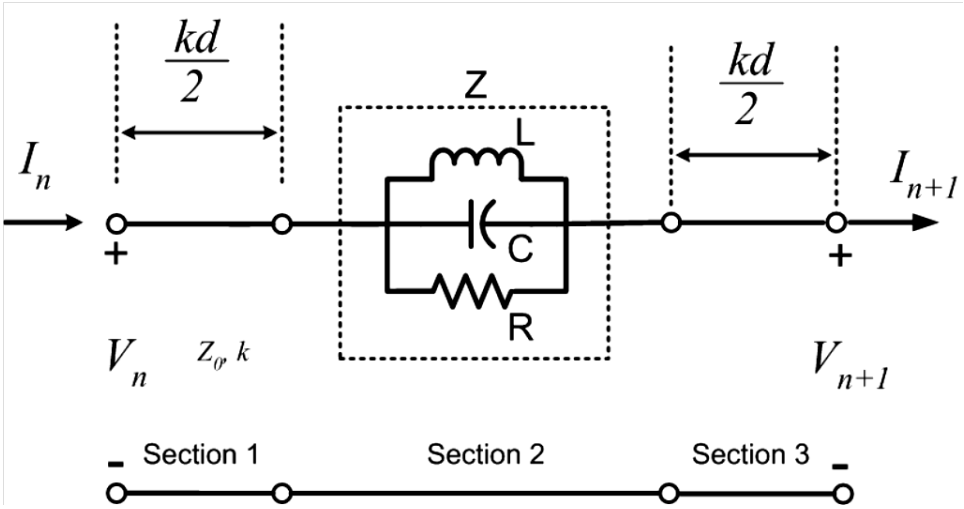

Figure 8: Equivalent Circuit Model of DGS loaded transmission line

$$R_i = 2Z_0\left(\frac{1}{|S_{21}(f_{0i})|} - 1\right) \quad \text{---------- (1)}$$

$$C_i = \frac{f_{C1}}{4\pi Z_0\left(f_{0i}{}^2 - f_{C1}{}^2\right)} \quad \text{---------- (2)}$$

$$L_i = \frac{1}{4\pi f_{0i}{}^2 C_i} \quad \text{---------- (3)}$$

$$\begin{bmatrix} A & B \\ C & D \end{bmatrix} = \begin{bmatrix} Cos\ \frac{kd}{2} & jZ_0\,Sin\ \frac{kd}{2} \\ jY_0\,Sin\ \frac{kd}{2} & Cos\ \frac{kd}{2} \end{bmatrix} \begin{bmatrix} 1 & Z \\ 0 & 1 \end{bmatrix} \begin{bmatrix} Cos\ \frac{kd}{2} & jZ_0\,Sin\ \frac{kd}{2} \\ jY_0\,Sin\ \frac{kd}{2} & Cos\ \frac{kd}{2} \end{bmatrix} \quad \text{---------- (4)}$$

where, $$Z = \frac{1}{\frac{1}{R} + \frac{1}{j\omega L} + j\omega C} \quad \text{---------- (5)}$$

$$S_{11} = \frac{A + B/Z_0 - CZ_0 - D}{A + B/Z_0 + CZ_0 + D} \quad \text{---------- (6)}$$

$$S_{21} = \frac{2(AD - BC)}{A + B/Z_0 + CZ_0 + D} \quad \text{---------- (7)}$$

Table I Equivalent Circuit Parameters

Parameters	CPW-ADGS BSF			
	Case 1	*Case 2*	*Case 3*	*Case 4*
f_{01} (GHz)	3.16	3.17	3.18	3.18
f_{02} (GHz)	3.34	3.40	3.42	3.45
f_{C1} (GHz)	2.69	2.73	2.75	2.76
R_1 (KΩ)	0.607	0.607	0.607	0.607
L_1 (nH)	1.6289	1.5059	1.4592	1.4224
C_1 (pF)	1.5569	1.6735	1.7162	1.7605
R_2 (KΩ)	2.71	1.158	0.9	0.531
L_2 (nH)	2.0785	2.071	2.0452	2.0757
C_2 (pF)	1.092	1.0578	1.0586	1.025

At resonant frequency, impedance of the any parallel *R*, *L*, and *C* resonance circuit is equals to *R* and the equivalent resistance at resonance condition is *R* equals to (R_1 + R_2). The radiation losses [Kim and Lee 2014] due to DGS have been calculated using (8). From (8), when the resistance goes to infinity (lossless), the radiation loss due to DGS becomes zero. Sharpness Factor (*SF*) [Smierzchalski, Kurgan, and Kitlinski 2010] is the measure of sharp rate of the filter cut-off, which has been calculated using (9). Filter selectivity (ξ) [Karmakar 2002] is the rate of the roll-off of the transfer function of the filter between the passband frequency (*fp*) and the stopband frequency (*fs)*. The smaller the difference between the passband and the stopband frequencies, the better is the selectivity, and it can be defined as (10). In (10), α_{max} is the 3 dB attenuation point, α_{min} is attenuation at f_0, $f_S = f_0$, and f_C is 3 dB cutoff frequency, where i = 1, for first resonance frequency (f_{01}) and i = 2, for second resonance frequency (f_{02}).

$$\eta = \frac{1}{\frac{R}{4Z_0}+\frac{Z_0}{R}+1} \quad \text{---------- (8)}$$

$$SF_i = \frac{f_{C1}}{f_{oi}} \quad \text{---------- (9)}$$

$$\xi_i = \frac{\alpha_{min} - \alpha_{max}}{f_{Si} - f_{pi}} \quad \text{---------- (10)}$$

The filter performance has been simulated using IE3D electromagnetic simulation tool and its results have been depicted in Figure 9. The theoretical filter characteristics have been evaluated after extracting as explained in preceding section. Comparison of simulated, theoretical and experimental results of proposed CPW bandstop filters are as shown in Figure 11. And the comparative performance analysis has been given in Table II. The performance analysis of all four configurations of CPW-BSF which has been carried out in terms of lower and upper cut-off frequencies at -3 dB i. e. f_{C1} and f_{C2} respectively, resonant frequencies at two transmission zeros i.e. f_{01} and f_{02} respectively, stop bandwidth (*SBW*) at -10 dB, attenuations at two transmission zeros i.e. α_1 and α_2 respectively, filter selectivity at lower and upper frequency sides of the stop band edges i. e. ξ_1 and ξ_2 respectively, sharp rate of cut-off at lower and upper frequency sides of the stop band edges i.e. sharpness factors SF_1 and SF_2 respectively given by (9) and radiation losses ($\% \eta$). From Table II, *Case 1* of CPW-ADGS BSF shows least radiation losses of 5.68 % and highest ξ_2 of 100 dB/GHz which is the best among *Case 2*, *Case 3*, and *Case 4*, and better than that reported in [Li 2014; Kulkarni et al. 2016].

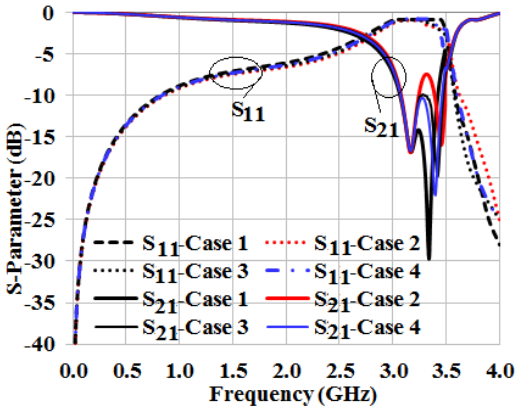

Figure 9: Comparision of S-parameters of the proposed cases of BSF

However, *Case 1* gives least ξ_1 and least *SBW* among *Case 2*, *Case 3*, and *Case 4*. It can be observed from Figure 9, the S_{21} plot of *Case 2* shows worse attenuation (< 10 dB) over a portion of stopband,

which results in least *SBW* among *Case 1*, *Case 3*, and *Case 4*. The *SBW* for *Case 3* is maximum among *Case 1*, *Case 2*, and *Case 4*, with lesser radiation loss than that of *Case 4*, and earlier reported work [Li 2014; Kulkarni et al. 2016], except ACPW-ADGS. Also, *Case 3* shows good ξ_1 and moderate ξ_2 values in comparisons with all the cases. The *Case 4* gives worst radiation loss (12.8 %) and least ξ_2 (48 dB/GHz) compared to all the cases. Good *SF* has been observed in all the cases studied and found close to the desired theoretical value of 1. Table II summarizes the comparative performance analysis of the BSF.

Table II Comparative Performance Analysis

Parameters	Ref. [Li 2014]			Ref. [Kulkarni et al. 2016]		CPW- BSF using proposed ADGS			
	CPW-DGS	*ACPW-DGS*	*ACPW-ADGS*	*CPW-SDGS*	*CPW-ADGS*	*Case 1*	*Case 2*	*Case 3*	*Case 4*
f_{C1} (GHz)	4.1			2.52		2.69	2.73	2.75	2.76
f_{C2} (GHz)	7.8	7.5	6.7	3.5		3.6	3.62	3.7	3.72
SBW (MHz)	300	350	900	300	340	350	390	430	420
% *FSBW*	5	5.55	15	9.37	10.6	10.76	11.87	13	12.66
f_{01} (GHz)	6	6.3	6	3.2		3.16	3.17	3.18	3.18
f_{02} (GHz)						3.34	3.40	3.42	3.45
α_1 (dB)	-14	-15.3	-25	-17.5	-23	-17	-17	-17	-17
α_2 (dB)						-29	-22	-20	-16
SF_1	0.68	0.65	0.68	0.78		0.85	0.861	0.864	0.867
SF_2	1.3	1.19	1.11	1.09		1.07	1.06	1.08	1.07
ξ_1 (dB /GHz)	5.78	5.59	11.57	21.32	29.41	29.8	32	32.6	33.3
ξ_2 (dB /GHz)	6.11	10.25	31.42	48.33	66.6	100	86.4	61	48
% η	31.9	28.4	10.6	23.1	13.1	5.68	10.1	11.6	12.8

This analytical study of CPW-BSF offers the fine alteration in fractional *SBW (FSBW)* from 10.76 % to 13 % with improvements on overall filter characteristics. Hence, from the foregoing discussion, it becomes apparent that *Case 3* is an optimum CPW-BSF using ADGS in terms of the overall performance, and hence it has been fabricated as shown in Figure 10, and tested on Vector Network Analyzer. Figure 11 shows that the measured filtering characteristics for the fabricated BSF are in good agreement with its simulated results.

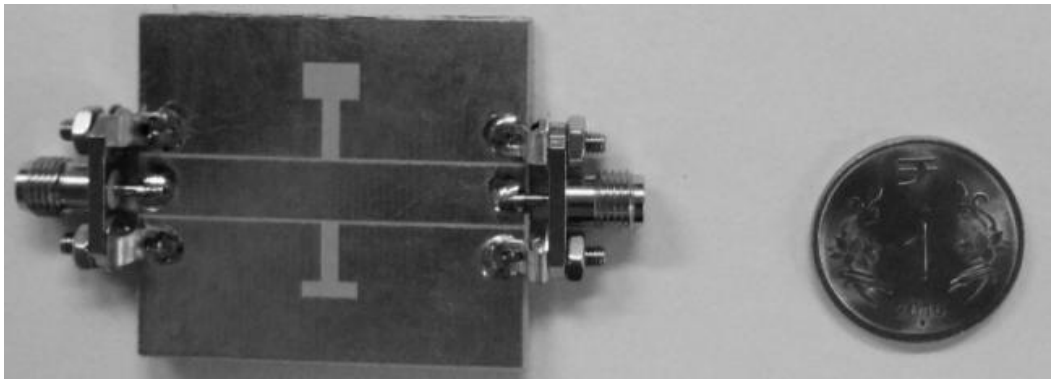

Figure 10: Photograph of fabricated CPW-BSF using proposed ADGS

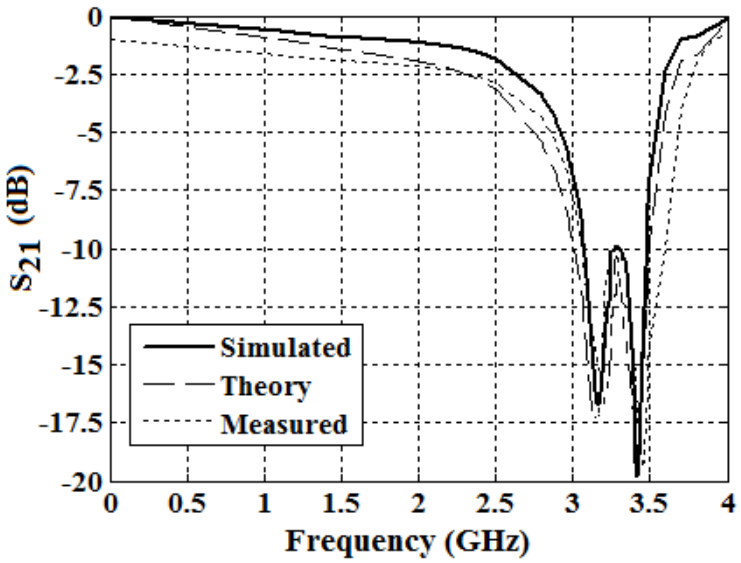

Figure 11: Comparision of simulated, theoretical (using *ABCD* matrix) and measured filter charactristic of proposed CPW- BSF

4. Conclusion

This work presents the design and analysis of four different cases of CPW-BSF using ADGS in order to achieve the fine alteration in stop band along with an overall improvement in filter characteristics as compared to earlier reported works. The comparative performance analysis of the all the proposed four cases of CPW-BSF shows that just by changing the width of proposed ADGS geometry the stop bandwidth can be varied over the range of 70 MHz with an improvement in other filter parameters like sharp rate of cut-off, filter selectivity, stopband attenuation, etc. The proposed geometry of ADGS is easy to design and circuit modeling to validate its theoretical response by method of evaluating the *ABCD* parameters. The measured performance of this novel design of fabricated CPW-BSF shows good agreement with its simulated and also the theoretical performance. The proposed CPW-BSF can be used as an alternative to the existing conventional BSF in many microwave and mobile portable devices.

Acknowledgement

The authors are thankful to Mr. Jagdish Prajapati and Mr. Prafull Irpache from RF and Microwave System (RFMS) Division, Society for Applied Microwave Electronics Engineering and Research (SAMEER), Mumbai, for their help in device fabrication and testing.

Reference

Ahn D., Park J. S., Park C. S., Kim J., Kim Y., Qian and T. Itoh, A design of the low-pass filter using the novel microstrip defected ground structure, *IEEE Trans. Microw. Theory Technique*, Vol. 49, no. 1, pp.86–93, Jan. 2001.

Chang Insik and Lee Bomson, Design of Defected Ground Structures for Harmonic Control of Active Microstrip Antenna, *Proc. Antennas and Propagation Society International Symposium*, San Antonio, USA, pp. 852 -855, August 2002.

Karmakar Nemai C., Improved performance of photonic band-gap microstrip structure with the use of chebyshev distributions, *Microwave Opt. Technol. Lett.*, Vol. 33, no. 1, pp. 01–05, Apr. 2002.

Kim Hyung-Mi, Lee Bomson, Bandgap and slow/fast wave characteristics of defected ground structures including left-handed features, *IEEE Trans. Microw. Theory Technique*, Vol. 54, no. 7, pp. 3113–3120, July. 2014.

Kulkarni Makarand G., Cheeran A. N., Ray K. P., and Kakatkar S. S., Design of a novel CPW filter using asymmetric DGS, *Proc. International Symposium on Antennas & Propagation*, Kochi, December 2016, pp. 13-16.

Kulkarni Makarand G., Cheeran A. N., Ray K. P., and Kakatkar S. S., Coplanar Waveguide Band Reject Filter Using Electromagnetic Band Gap Structure, *Progress In Electromagnetics Research Lett.*, Vol. 70, pp. 53–58, Sept. 2017.

Li Xiaoming, Asymmetric Coplanar Waveguide Filter with Defected Ground Structure, *Proc. XXXIth General Assembly and Scientific Symposium*, URSI GASS, pp. 1–4, 2014,.

Lim Jong-Sik, Kim Chul-Soo, Lee Young-Taek, Ahn Dal, and Nam Sangwook, A Spiral-Shaped Defected Ground Structure for Coplanar Waveguide, *IEEE Microw. Wireless Compon. Lett.*, Vol. 12, no.9, pp.330–332, Sept. 2002.

Lin Shui-Yang, Tian Wei-Zhong, Zheng Shu-Qi, and Sun Xiao-Wei, A Semicircle DGS With High Q Factor for Microstrip Line and Low-Pass Filter, *Proc. APMC'2006*, Yokohama, Japan, pp. 1197–1199, December 2006.

Martine F., Falcone F., Bonache J., Lopetegi T., Laso M., and Sorolla M., Dual electromagnetic band gap CPW structures for filter applications, *IEEE Microw. Wireless Compon. Lett.*, Vol. 13, no.9, pp.393–395, Sept. 2003.

Naqui Jodi, Su Lijuan, Mata Javier, and Martin Ferran, Coplanar waveguides loaded with symmetric and asymmetric pairs of slotted stepped impedance resonators: Modeling, applications, and comparison to SIR-loaded CPWS, *Microwave Opt Technol Lett.*, Vol. 58, no. 11, pp. 2741–2745, Nov. 2016.

Pozar David M., 2010, third edition, *Microwave Engineering*, pp.412-415 (John Wiley & Sons, New Delhi)

Smierzchalski M., Kurgan P., and Kitlinski M., Improved selectivity compact band-stop filter with gosper frcatal-shaped defected ground structures, *Microwave Opt. Technol. Lett.*, Vol. 52, no. 1, pp. 227–229, Jan. 2010.

Wen C. P., Coplanar waveguide: A surface strip transmission line suitable for nonreciprocal gyro-magnetic device applications, *IEEE Trans. Microw. Theory Technique*, Vol. 17, no. 12, pp.1087–1090, Dec. 1969.

Yun T.Y. and Chang K., Uniplanar one-dimentional photonic bandgap structures and resonators, *IEEE Trans Microw. Theory Tech.*, Vol. 49, no. 3, pp. 549 -553, Mar.2001.

Zoul Yongzhuo, Hu Xin, He Sailing ,and Lin Zhili, Compact coplanar waveguide lowpass filter using a novel electromagnetic bandgap structure, *Proc. International Symposium on Antennas Propagation & EM Theory*, Guilin, China, pp. 01–04, October 2006.